IEEE Access
Multidisciplinary ⋮ Rapid Review ⋮ Open Access Journal

Received February 2, 2021, accepted March 8, 2021, date of publication March 19, 2021, date of current version March 29, 2021.

Digital Object Identifier 10.1109/ACCESS.2021.3067458

Towards Turning Smartphones Into mmWave Scanners

GUILLERMO ÁLVAREZ-NARCIANDI, JAIME LAVIADA, AND FERNANDO LAS-HERAS, (Senior Member, IEEE)
Department of Electrical Engineering, University of Oviedo, 33203 Gijón, Spain

Corresponding author: Guillermo Álvarez-Narciandi (alvareznguillermo@uniovi.es)

This work was supported in part by the Ministerio de Ciencia, Innovación y Universidades of Spain /FEDER under Project RTI2018-095825-B-I00, and in part by the Gobierno del Principado de Asturias under Project GRUPIN-IDI-2018-000191.

ABSTRACT This paper aims to assess the possibilities of using current and incoming fifth generation (5G) devices as millimeter wave (mmWave) imagers. For this purpose, previous works about freehand scanning with compact devices working at mmWave frequencies are herein extended. In particular, a new tracking unit is now attached to the scanning device so the main parts of the freehand imager, namely the radiofrequency (RF) and tracking subsystems, become portable and not depend on external systems. Specifically, this work illustrates the possibilities of 5G devices working at the mmWave band as imagers. Results supporting that the embedded tracking unit provides enough accuracy are described and compared with an accurate reference system. The impact of the final image is also considered revealing that the shape of imaged objects can be easily identified.

INDEX TERMS Freehand imaging, real-time imaging, mmWave imaging, handheld scanner, synthetic aperture radar (SAR), position tracking, irregular sampling, 5G.

I. INTRODUCTION

The advent of fifth generation (5G) technology [1] has brought a new set of outstanding features to our hands, being low-latency and higher bandwidth the flagship characteristics. Nevertheless, recent advances on freehand millimeter wave (mmWave) imaging [2] have opened up a new horizon of possibilities for almost any device with mmWave capabilities, envisaging new uses for 5G devices.

Freehand mmWave imaging is a novel technique, which is able to generate an electromagnetic image with capacity to see through certain materials such as paperboard, smoke or clothing by just doing arbitrary traces with our hand over the volume to be imaged. This flexibility, which is coupled to the use of compact devices, is a key feature of all freehand systems, which have also been used for other applications such as ultrasound medical imaging [3], [4], direct mapping of electromagnetic sources in the context of electromagnetic compatibility [5], or antenna measurement [6].

Freehand mmWave imaging is based on conventional synthetic aperture radar (SAR) imaging [7], [8] and it requires two main components: i) a radiofrequency (RF) unit working at mmWave frequencies with capacity to transmit and receive signals, and ii) a tracking unit to follow the position of the RF unit.

Currently, freehand mmWave imaging has been demonstrated using compact radar units at 60 GHz, though positioning depends on an external tracking system based on a motion capture system [2], [9]. Despite the tracking system can be easily and quickly deployed and calibrated, it still prevents the development of fully compact devices with freehand imaging capabilities.

The deployment of 5G New Radio (5G NR) systems [10], which consider frequencies along multiple mmWave subbands, brings a new set of potential *RF units* which will be used in multiple end-user compact devices. Moreover, the communications systems at those frequencies are expected to provide multibeam capabilities to obtain increased energy efficiency, reduced interference levels and more secure communications. These multibeam capabilities are provided by Multiple-Input-Multiple-Output (MIMO) systems, which are very convenient for imaging purposes as discussed next [11]. In addition, in the last years, advances in telecommunications devices are not only inherent to moving to new communication generations (e.g, 5G) but also to the subsystems embedded in these devices, being some of them very related to the

The associate editor coordinating the review of this manuscript and approving it for publication was Zihuai Lin.

technology considered in this paper. For instance, mmWave radars have been developed [12] for gesture detection [13]. These radars also include MIMO capabilities, which have been recently exploited for freehand mmWave imaging [9]. Thus, RF units in modern communication devices exhibit a number of features that are outstanding for freehand mmWave imaging.

On the other hand, regarding the *tracking unit*, several approaches based on 5G technology are available (e.g., [14]) exploiting the new options of the communication standard. Nevertheless, they are still far from providing a subwavelength accuracy at mmWave frequencies as required by freehand systems [2], [9]. Other technologies available in modern devices, such as the latest versions of Bluetooth including angle-of-arrival detection capabilities [15] and the well-known Global Navigation Satellite System (GNSS) do not provide subwavelength accuracy either.

However, modern devices have started to include arrays of conventional cameras, or RGB sensors, for photography purposes. Despite it is not their main goal, these arrays provide multiview capabilities enabling positioning tracking by exploiting stereo vision or photogrammetry [16]. Furthermore, extended RGB cameras, such as those that also measure depth (also known as RGB-D or depth cameras), are becoming available for assisting some systems in tasks such as face recognition and virtual reality applications. RGB and RGB-D sensors have already been used in some portable electromagnetic systems [17]–[19]. Nevertheless, none of those systems are as compact as those considered in the case of freehand mmWave imaging, which aims to use *pocket-size* devices for electromagnetic imaging purposes.

Thus, current RF and tracking systems for incoming smartphones are very promising in order to implement a compact freehand imager easily driven by hand. Moreover, the fact that all the required components to build a freehand mmWave imaging system, or similar ones, can be already found in modern smartphones is a clear indicator that the power consumption, though not negligible, is affordable.

Other mmWave imaging approaches, which yield systems that are either not portable or not compact enough to be driven by hand are discussed below. In addition, their main features and those of freehand mmWave imaging systems are summarized in Table 1.

Some systems are based on inverse scattering methods, which pursue to inversely solve the Maxwell equations [20]. Although these methods enable to solve problems with high accuracy, allowing subwavelength problem analysis, they entail a high computational burden, which typically prevents real-time applications. In this regard, the adoption of machine learning techniques to deliver real-time results employing inverse scattering methods (at least for tomography schemes) is being investigated [21]–[23]. In addition, only electrically small problems are considered to mitigate ill-conditioning.

Instead, traditional SAR imaging systems are less computationally demanding at the expense of a lower resolution, which depends on the scanning aperture. Thus, to achieve a high resolution, these systems must rely on large physical or synthetic apertures. Booth-size systems, like those used at airports [8], [24], employ a high number of transmitters and receivers to obtain dense arrays to build large physical apertures. It should be noted that the number of transmitters and receivers can be reduced using MIMO configurations [11]. These systems generate a high data throughput and, consequently, a few seconds may be required to retrieve the final electromagnetic image.

TABLE 1. Comparison of mmWave imaging techniques.

System type	Device size	Overall speed	Electrical object size	Resolution	Comp. burden
Tomography inverse scattering [20]	Medium	Not real-time	Small	High	High
Booth-size scanner [8], [24]	Large	Quasi real-time	Large	Medium	Medium
Microwave camera [25], [26]	Medium	Real-time	Large	Medium	Low
Freehand scanner [2], [9], [This work]	Small	Real-time	Large	Medium	Low

A trade-off between size and resolution was achieved with the microwave cameras presented in [25], [26] which, though portable, were still rather bulky. These devices also rely on a physical aperture but with a much smaller size at the expense of some resolution loss, which is partially compensated by a shorter stand-off distance. Moreover, the reduced amount of data enables real-time applications. An alternative system of reduced size, when high-fidelity images are not required, has also been proposed in [27] by exploiting the concept of chaotic excitation SAR. Other systems take advantage of the movement of targets to use inverse SAR techniques [28].

Compared to the previous approaches, freehand mmWave imaging techniques are a further evolution in terms of compactness as they are based on a small number of transmitters and receivers which is synthetically increased by arbitrarily moving the handheld device. Therefore, high-resolution images with a significantly compact RF unit are obtained employing data acquired across different positions, increasing the overall acquisition time when compared with systems exploiting large physical (i.e., non-synthetic) apertures. Moreover, the image can be updated on real-time with a very low computational burden as more measurements are acquired. Thus, this kind of systems provides a trade-off between compactness and image quality, which is convenient for some applications such as those requiring the inspection of areas that may not be reachable with a bulky scanner.

In addition, compared to the previous approaches, freehand mmWave imagers are more flexible as, thanks to the real-time feedback, the user can decide on-the-fly in which part of the area of interest may be necessary to perform more acquisitions.

This manuscript hybridizes the current freehand mmWave imaging systems [2], [9] with an autonomous stereoscopic system avoiding the need of external tracking and, therefore,

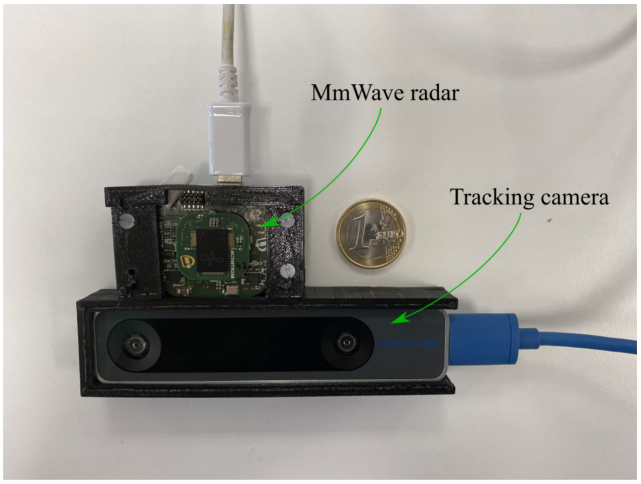

FIGURE 1. MmWave imager formed by a compact radar-on-chip module and a tracking camera.

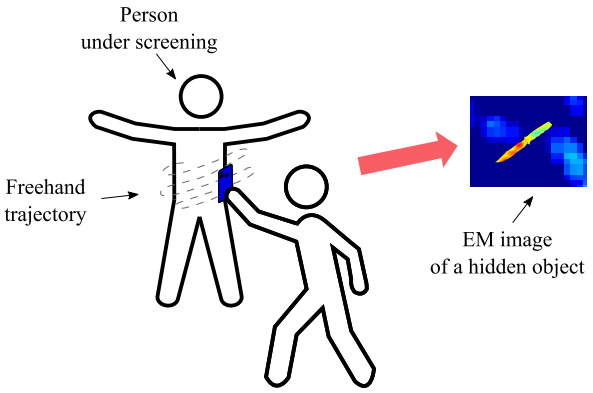

FIGURE 2. Scheme of the proposed imaging system.

overcoming the main limitation to achieve a *compact freehand mmWave imager*. In fact, this is a milestone in the path towards taking advantage of the sensors integrated in mass-market general purpose devices, such as smartphones, to develop a handheld imaging scanner.

The rest of this paper is structured as follows. First, the system architecture is presented in Section II. Then, the imaging technique is discussed in Section III. Next, in Section IV measurement results obtained with the proposed handheld scanner are presented and compared with reference ones and the positioning accuracy reached with the tracking camera is discussed. Finally, the conclusions are drawn in Section V.

II. SYSTEM ARCHITECTURE

The architecture of the proposed system is an evolution of the systems presented in [2], [9], where the concept of freehand radar imaging was introduced. In both cases, the systems relied on external infrastructure to obtain the position of the radar at each acquisition, allowing the coherent combination of different measurements. In particular, an optical tracking system comprising several infrared cameras was employed. Instead, in the proposed system a stereoscopic tracking camera is used to track the radar along a freehand trajectory, which paves the way to embed the whole mmWave scanner into a single device, as it can be seen in Fig. 1.

An application example of the proposed system, security screening, is depicted in Fig. 2. As it can be observed, the user of the system moves the scanner, which does not rely on external infrastructure, with their hand while radar acquisitions are performed. These measurements are coherently combined using the tracking information provided by the sensors included in the scanner, in this case a stereoscopic camera, to generate high-resolution images in *real-time*.

The system is structured in three parts: radar subsystem, positioning subsystem and control and processing subsystem.

In order to achieve a good resolution, the radar subsystem should work at the mmWave band. This could be achieved by using either a dedicated RF unit integrated in the device in which the handheld scanner is embedded, or by using a RF unit already available in the device, e.g. the communications module of a smartphone or a general purpose radar unit. In this implementation, the module BGT60TR24B by Infineon® [12], which is a frequency-modulated continuous-wave (FMCW) radar-on-chip module available in some smartphone models for gesture detection [29], is used. This radar module transmits a signal with a frequency waveform describing an up-chirp saw tooth pattern centered at $f_c = 60\,\text{GHz}$ with a bandwidth of $BW = 6\,\text{GHz}$ and a chirp duration of $T_s = 512\,\mu\,\text{s}$. The scanner employs the two transmitters of the radar module, which are activated sequentially, and its four receivers, which perform dechirp-on-receive operations concurrently.

The positioning subsystem is formed by the Intel® RealSense™ tracking camera T265 [30]. This subsystem is based on an array of two RGB sensors together with an inertial measurement unit (IMU) comprising three-axis accelerometers and gyroscopes. Once again, similar sensors can be found in current smartphones and, thus, analogous tracking capabilities are envisaged for incoming smartphone generations.

Finally, the control and processing subsystem is in charge of triggering the radar and position acquisitions, and of processing the acquired data to retrieve high-resolution electromagnetic images of the investigation domain. These images are displayed to the operator of the scanner in real-time. In a final implementation, this subsystem can be either entirely implemented in the portable device, or a distributed architecture can be adopted. For instance, the subsystem to control the radar and tracking subsystems can be embedded while the acquired data is sent to another device (e.g., a PC), which implements the imaging algorithm (i.e., does the processing). The final choice depends on the computational capabilities of the portable device. In this demonstrator, in order to get a flexible testing environment, the entire control and processing subsystem is implemented with a laptop which interfaces via USB to the radar and the positioning subsystems. It should be remarked that this simplification does not have an impact in the final results as the input data is the same.

The information obtained from the radar and positioning subsystems is processed in two steps. First, a strategy to ensure a proper sampling to cope with the handheld operation of the scanner is implemented. Second, the resulting data is used to compute the reflectivity of the investigation domain as discussed in Section III. Regarding the first step, it should be kept in mind that, since the scanner is moved by hand while data is acquired, the obtained samples will not be uniformly spaced. Moreover, the irregular hand movements would yield an uneven sampling distribution unless a technique to avoid locally oversampled areas, which may cause image artifacts, is implemented. To overcome this, in the proposed system, in a similar fashion to [2], [9], an observation domain is defined over the inspected area. This observation domain is a three-dimensional (3D) volume, designed to mimic a planar acquisition grid of a traditional imaging system. It is discretized in cubic cells within which only a maximum of Q acquisitions are allowed. After Q samples are acquired within a cell, if additional measurements are performed the extra acquisitions are discarded. Additionally, acquisitions performed outside the observation domain, i.e., outside the 3D volume defined by the cells, are also dismissed. It should be noted that the sampling rate can be controlled by modifying the size of the cells, which also defines the upper bound of the maximum gap between adjacent samples.

III. IMAGING TECHNIQUE

The handheld scanner yields a non-uniform distribution of radar acquisitions. Moreover, it is desired to obtain a real-time feedback of the image of the investigation domain so that the operator can decide how to proceed with the scan. Therefore, instead of resorting to widespread accelerated SAR techniques for monostatic or multistatic setups [8], [11], [31], a flexible delay-and-sum (DAS) algorithm, adapted to FMCW radar signals, is employed [9] at the expense of a reduced computational efficiency when compared to Fast Fourier Transforms (FFT) based methods [31], [32]. Thus, the reflectivity from each point of the investigation domain, $\mathbf{r}'$, at the m-th radar acquisition can be expressed as:

$$\rho_m(\mathbf{r}') = \sum_{i=1}^{m} \sum_{p=1}^{nrx} \sum_{n=1}^{ntx} s_{c,i,p,n}\left(\mathbf{r}', \frac{BW}{T_s}\frac{R_{i,p}+R_{i,n}}{c}\right), \quad (1)$$

where nrx and ntx are the number of receivers and the number of transmitters of the radar module, respectively; $R_{i,p}$ is the distance from the p-th receiver of the radar at the i-th radar acquisition to $\mathbf{r}'$ and $R_{i,n}$ is the distance from the n-th transmitter of the radar at the i-th radar acquisition to $\mathbf{r}'$; and $s_{c,i,p,n}$ is given by

$$s_{c,i,p,n}(\mathbf{r}', f) = \mathscr{F}\left\{ s_{IF,i,p,n}(t) e^{-j2\pi f_c \frac{R_{i,p}+R_{i,n}}{c}} \right\}, \quad (2)$$

where $\mathscr{F}\{\cdot\}$ denotes the Fourier transform operator and $s_{IF,i,p,n}$ is the analytic signal computed by means of a Hilbert transform [33] from the dechirped-on-receive signal retrieved by the p-th receiver of the radar module. As it can be observed in Eq. (1), it is straightforward to update the reflectivity of each point of the investigation domain on-the-fly as more acquisitions are performed.

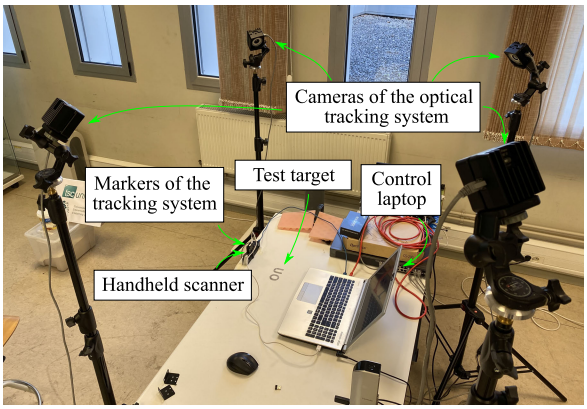

FIGURE 3. Measurement setup used to assess the imaging performance of the handheld scanner.

IV. RESULTS

To assess the performance of the proposed handheld scanner several tests were carried out. For that purpose, different test targets were measured performing a handheld scan and the retrieved images were compared with those obtained using a reference tracking system. In particular, the reference images were obtained employing the position and attitude data from the scanner measured with a high-accuracy infrared optical tracking system [34], which will be considered as the ground-truth, to coherently combine the radar acquisitions. In this case, the optical tracking system consisted of four infrared cameras, which were deployed and calibrated in the area were the targets were placed, and four reflective markers attached to the handheld scanner which were used by the cameras to track its position (Fig. 3).

First, the positioning accuracy provided by the tracking camera for a sample trajectory is analyzed. For that purpose, the position data retrieved by the tracking camera included in the handheld scanner during the scan is compared with that given by the external infrared motion capture system. The results are shown from Fig. 4a to Fig. 4c. As it can be inferred from these figures, during the scan the operator described an *s-shape* trajectory with the handheld scanner in which the main movement axis was the *x-axis*. In addition, the axis orthogonal to the test target, i.e., the *depth* axis, was the *z-axis*. The root-mean-squared positioning error in the *x-axis*, in the *y-axis* and in the *z-axis* are 0.9 mm, 0.5 mm and 0.8 mm, respectively. To ease the assessment of the positioning errors during the scan, the empirical cumulative distribution function (ECDF) of the error in each axis is depicted in Fig. 4d. As it can be seen, in 90% of the cases the error is below 0.8 mm in the *z-axis*, below 1.3 mm in the *y-axis*, and below 1.4 mm in the *x-axis*. Although these errors are not negligible from the electromagnetic point of view, the errors are locally smaller, i.e., sometimes the tracking camera position

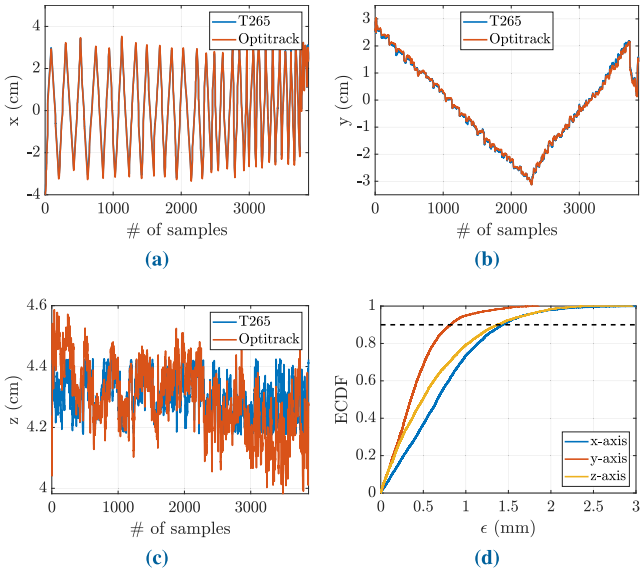

FIGURE 4. Positioning data obtained from the tracking camera included in the handheld scanner and from the external infrared motion capture system: *x-axis* (a), *y-axis* (b), and *z-axis* (c). ECDF of the positioning errors in each axis (d).

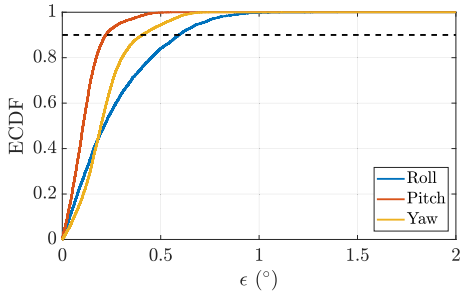

FIGURE 5. ECDF of the error of attitude estimations during the sample trajectory for the yaw, pitch and roll angles.

estimations drift slightly until the camera is able to relocalize itself, but the relative error between adjacent samples is not as high as its absolute value. Therefore, the coherence of the measurements is only slightly degraded. Regarding the different positioning error values of each axis, it should be mentioned that the higher errors correspond to the movement axis, i.e., the *x-axis*. In addition, the errors in the depth axis, i.e., the *z-axis*, are higher as the tracking camera provides a slightly less accuracy in that axis.

The attitude estimations provided by the tracking camera are also compared with the data obtained with the external infrared motion capture system. In particular, the ECDF of the error of the attitude estimations of the tracking camera during the sample trajectory for the yaw, pitch and roll angles is depicted in Fig. 5. As it can be seen, the accuracy is significantly high, being the error value for every attitude angle below 1° in more than 90% of the cases.

For the first scan performed to retrieve an electromagnetic image, it was decided to use the star pattern with a 2.5 cm radius and six spokes shown in Fig. 6a, which was made of metal, as test target. Within the scan a total

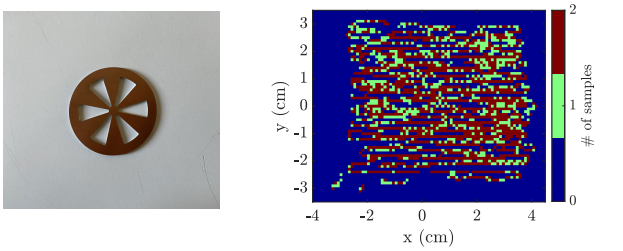

FIGURE 6. Star pattern used as test target (a) and distribution of acquired samples projected onto a 2D grid (b).

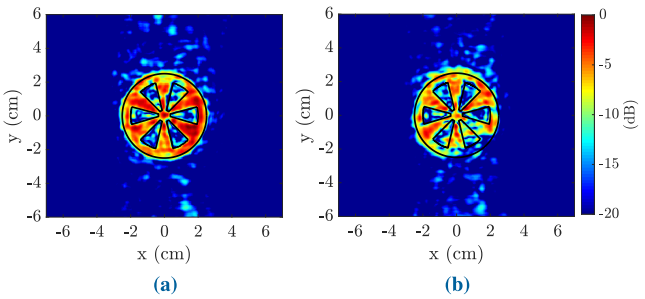

FIGURE 7. Reference reflectivity image obtained using the infrared motion capture system (a) and reflectivity image retrieved with the proposed handheld scanner (b).

of 3872 acquisitions were performed during 522 s at an average distance from the target of 4.3 cm. The distribution of the acquired samples, projected onto a two-dimensional (2D) grid formed by the cross-section of the cells in which the observation domain was discretized, is depicted in Fig. 6b.

The reference reflectivity image, obtained considering the positioning data from the infrared optical tracking system, is depicted in Fig. 7a and the reflectivity image obtained with the handheld scanner is shown in Fig. 7b. As it can be seen, overall, in both cases the shape of the star pattern is well-reconstructed. However, the quality of the bottom-right part of the target in the image obtained with the handheld scanner was degraded due to higher positioning errors in that area, which caused a degradation in the coherency of the measurements.

In order to quantitatively assess the quality loss of the reflectivity image retrieved with the handheld scanner compared to the reference one, the target-to-clutter ratio (TCR) [35], [36] was computed. The TCR is given by

$$TCR = 10 \log \left(\frac{N_c \sum_{(x,y)\in A_t} |\rho(x,y)|^2}{N_t \sum_{(x,y)\in A_c} |\rho(x,y)|^2} \right), \tag{3}$$

where A_t is the region corresponding to the target (i.e. the pixels where the target is located), A_c is the rest of the image, N_t is the number of pixels of A_t and N_c is the number of pixels of A_c. The obtained TCR value of the reference image and the one obtained with the handheld scanner are 16.5 and 14.5 dB, respectively, i.e., there is only a 2 dB loss.

For the second test it was decided to use the metal letter depicted in Fig. 8a as test target. In this test a total of 3198 acquisitions were performed during 347 s at an average

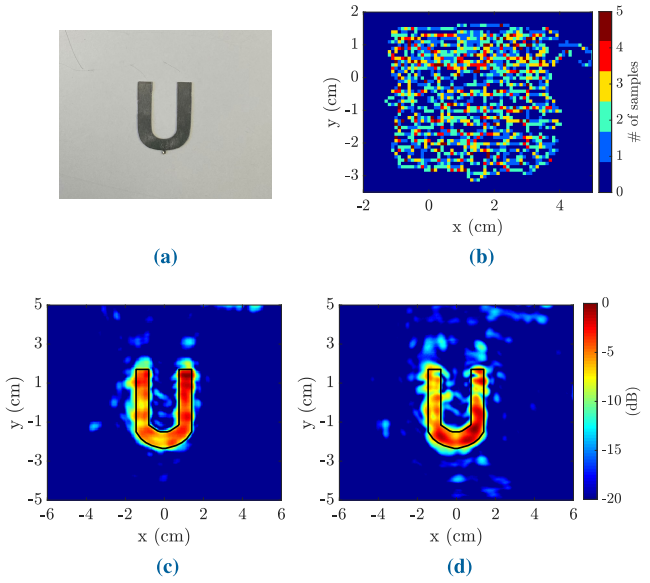

FIGURE 8. Image of the letter used as test target (a), distribution of acquired samples projected onto a 2D grid (b), reference reflectivity image obtained using the infrared motion capture system (c) and reflectivity image retrieved with the proposed handheld scanner (d).

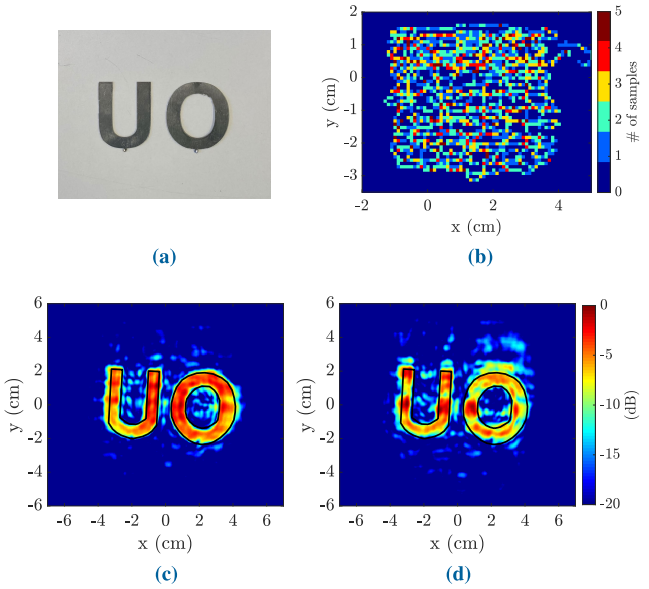

FIGURE 9. Image of the letters used as test target (a), distribution of acquired samples projected onto a 2D grid (b), reference reflectivity image obtained using the infrared motion capture system (c) and reflectivity image retrieved with the proposed handheld scanner (d).

distance of 6.2 cm from the target. The distribution of the acquired samples is shown in Fig. 8b. The reference reflectivity image, obtained considering the positioning data from the infrared optical tracking system, is depicted in Fig. 8c and the reflectivity image obtained with the handheld scanner is shown in Fig. 8d. As it can be observed, the shape of the objects, plotted with a black-solid line, is well-reconstructed in both cases, being the image obtained with handheld scanner slightly noisier than the reference one. The TCR of the reference image is 16.8 dB and that of the image computed with the handheld scanner is 15.5 dB, i.e., only a 1.3 dB difference.

Next, a second letter was added to the test target to form the acronym of the University of Oviedo (Fig. 9a). During the scan, which lasted 583 s, 5093 samples were acquired at an average distance of 6.1 cm from the test target. The reference reflectivity image, obtained considering the positioning data from the infrared optical tracking system, is shown in Fig. 9c and the reflectivity image obtained with the handheld scanner can be observed in Fig. 9d. As it can be seen, the shape of both letters, plotted with a black-solid line, matches with high accuracy the shape of test target in both cases, being the image obtained with handheld scanner slightly noisier than the reference one. In this case, the TCR of the reference image is 16.0 dB and that of the image computed with the handheld scanner is 14.1 dB.

The acquisitions performed to scan the different targets and the TCR of the retrieved images are summarized in Table 2, where the TCR of the reference image and that of the image obtained with the handheld scanner are denoted by TCR_{ref} and TCR_{hand}, respectively.

Finally, in order to show a 3D image, one of the letters of the previous test target was placed on top of a foam base so

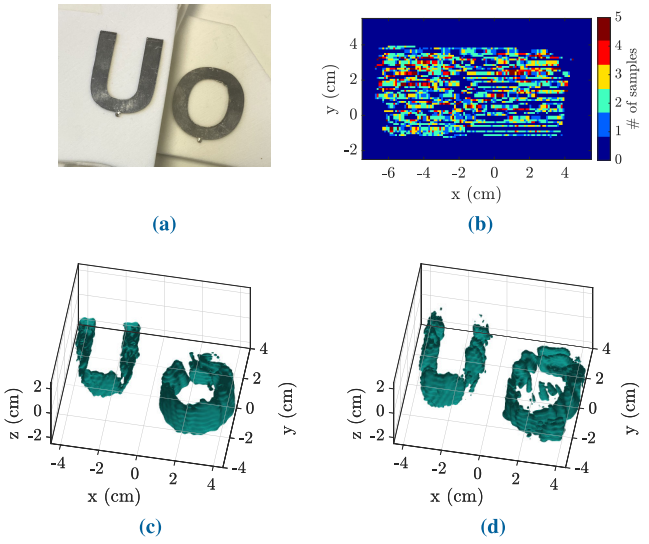

FIGURE 10. Image of the letters used as test target placed at different height (a), distribution of acquired samples projected onto a 2D grid (b), profile reconstruction of the normalized reflectivity isosurface corresponding to −9 dB of both targets obtained using the infrared motion capture system (c) and retrieved with the proposed handheld scanner (d).

TABLE 2. Summary of the measurement results reported from Fig. 6 to Fig. 9.

Target	# of samples	Avg. dist. to target (cm)	Time (s)	TCR_{ref} (dB)	TCR_{hand} (dB)
Star pattern	3872	4.3	522	16.5	14.5
"U"	3198	6.2	347	16.8	15.5
"UO"	5093	6.1	583	16.0	14.1

it was located 3 cm higher than the other letter (see Fig. 10a). The distribution of the 4867 samples acquired during the scan can be observed in Fig. 10b. The average distance from the

acquisition positions to the targets was 4.5 cm in the case of the letter "U" and 7.5 cm for the letter "O" and the total acquisition time was 591 s. The profile reconstruction of the normalized reflectivity isosurface corresponding to −9 dB of both targets obtained with the motion capture system is shown in Fig. 10c, and that retrieved with the handheld scanner is depicted in Fig. 10d. Analogously to the previously presented results, the shape of both targets is well-reconstructed.

V. CONCLUSION

In this manuscript, a compact handheld imager is presented. The presented scanner hybridizes a state-of-the-art freehand imaging system with an stereoscopic camera capable of performing simultaneous localization and mapping, enabling the coherent combination of radar measurements to obtain high-resolution images without the need of external tracking infrastructure. The proposed system paves the way to the development of mmWave scanners leveraging the sensors included in modern smartphones, opening a wide-range of applications.

The performance of the proposed handheld scanner has been extensively evaluated through different measurements, and the achieved results were compared with those retrieved considering the tracking information provided by a high-accuracy infrared motion capture system, showing that, although the reflectivity images obtained with the presented handheld scanner are slightly noisier than the reference ones, the quality is still good.

REFERENCES

[1] T. S. Rappaport, S. Sun, R. Mayzus, H. Zhao, Y. Azar, K. Wang, G. N. Wong, J. K. Schulz, M. Samimi, and F. Gutierrez, "Millimeter wave mobile communications for 5G cellular: It will work!," *IEEE Access*, vol. 1, pp. 335–349, 2013.

[2] G. Alvarez-Narciandi, M. Lopez-Portugues, F. Las-Heras, and J. Laviada, "Freehand, agile, and high-resolution imaging with compact mm-wave radar," *IEEE Access*, vol. 7, pp. 95516–95526, 2019.

[3] L. Mercier, T. Langø, F. Lindseth, and L. D. Collins, "A review of calibration techniques for freehand 3-D ultrasound systems," *Ultrasound Med. Biol.*, vol. 31, no. 2, pp. 143–165, Feb. 2005.

[4] M. H. Mozaffari and W.-S. Lee, "Freehand 3-D ultrasound imaging: A systematic review," *Ultrasound Med. Biol.*, vol. 43, no. 10, pp. 2099–2124, Oct. 2017.

[5] H. He, P. Maheshwari, and D. J. Pommerenke, "The development of an EM-field probing system for manual near-field scanning," *IEEE Trans. Electromagn. Compat.*, vol. 58, no. 2, pp. 356–363, Apr. 2016.

[6] G. Alvarez-Narciandi, J. Laviada, Y. Alvarez-Lopez, and F. Las-Heras, "Portable freehand system for real-time antenna diagnosis and characterization," *IEEE Trans. Antennas Propag.*, vol. 68, no. 7, pp. 5636–5645, Jul. 2020.

[7] J. M. Lopez-Sahcnez and J. Fortuny-Guasch, "3-D radar imaging using range migration techniques," *IEEE Trans. Antennas Propag.*, vol. 48, no. 5, pp. 728–737, May 2000.

[8] D. M. Sheen, D. L. Mcmakin, and T. E. Hall, "Three-dimensional millimeter-wave imaging for concealed weapon detection," *IEEE Trans. Microw. Theory Techn.*, vol. 49, no. 9, pp. 1581–1592, Sep. 2001.

[9] G. Alvarez-Narciandi, J. Laviada, and F. Las-Heras, "Freehand mm-wave imaging with a compact MIMO radar," *IEEE Trans. Antennas Propag.*, vol. 69, no. 2, pp. 1224–1229, Feb. 2021.

[10] 3GPP. (Jan. 2021). *3GPP Specification Series: 38Series*. [Online]. Available: https://www.3gpp.org/DynaReport/38-series.htm

[11] S. S. Ahmed, A. Schiessl, and L.-P. Schmidt, "A novel fully electronic active real-time imager based on a planar multistatic sparse array," *IEEE Trans. Microw. Theory Techn.*, vol. 59, no. 12, pp. 3567–3576, Dec. 2011.

[12] I. Nasr, R. Jungmaier, A. Baheti, D. Noppeney, J. S. Bal, M. Wojnowski, E. Karagozler, H. Raja, J. Lien, I. Poupyrev, and S. Trotta, "A highly integrated 60 GHz 6-Channel transceiver with antenna in package for smart sensing and short-range communications," *IEEE J. Solid-State Circuits*, vol. 51, no. 9, pp. 2066–2076, Sep. 2016.

[13] J. Lien, N. Gillian, M. E. Karagozler, P. Amihood, C. Schwesig, E. O. H. Raja, and I. Poupyrev, "Soli: Ubiquitous gesture sensing with millimeter wave radar," *ACM Trans. Graph.*, vol. 35, no. 4, p. 142, 2016.

[14] H. Wymeersch, G. Seco-Granados, G. Destino, D. Dardari, and F. Tufvesson, "5G mmWave positioning for vehicular networks," *IEEE Wireless Commun.*, vol. 24, no. 6, pp. 80–86, Dec. 2017.

[15] Z. Hajiakhondi-Meybodi, M. Salimibeni, K. N. Plataniotis, and A. Mohammadi, "Bluetooth low energy-based angle of arrival estimation via switch antenna array for indoor localization," in *Proc. IEEE 23rd Int. Conf. Inf. Fusion (FUSION)*, Jul. 2020, pp. 1–6.

[16] R. Hartley and A. Zisserman, *Multiple View Geometry in Computer Vision*, 2nd ed. Cambridge, U.K.: Cambridge Univ. Press, 2003.

[17] J. Laviada, A. Arboleya-Arboleya, Y. Álvarez, B. González-Valdés, and F. Las-Heras, "Multiview three-dimensional reconstruction by millimetre-wave portable camera," *Sci. Rep.*, vol. 7, no. 1, pp. 1–11, Dec. 2017.

[18] J. Laviada, M. Lopez-Portugues, A. Arboleya-Arboleya, and F. Las-Heras, "Multiview mm-wave imaging with augmented depth camera information," *IEEE Access*, vol. 6, pp. 16869–16877, 2018.

[19] J. Laviada, M. T. Ghasr, M. Lopez-Portugues, F. Las-Heras, and R. Zoughi, "Real-time multiview SAR imaging using a portable microwave camera with arbitrary movement," *IEEE Trans. Antennas Propag.*, vol. 66, no. 12, pp. 7305–7314, Dec. 2018.

[20] M. T. Bevacqua, S. Di Meo, L. Crocco, T. Isernia, and M. Pasian, "Millimeter-waves breast cancer imaging via inverse scattering techniques," *IEEE J. Electromagn., RF Microw. Med. Biol.*, early access, Jan. 15, 2021, doi: 10.1109/JERM.2021.3052096.

[21] Z. Wei and X. Chen, "Deep-learning schemes for full-wave nonlinear inverse scattering problems," *IEEE Trans. Geosci. Remote Sens.*, vol. 57, no. 4, pp. 1849–1860, Apr. 2019.

[22] K. Xu, L. Wu, X. Ye, and X. Chen, "Deep learning-based inversion methods for solving inverse scattering problems with phaseless data," *IEEE Trans. Antennas Propag.*, vol. 68, no. 11, pp. 7457–7470, Nov. 2020.

[23] X. Ye, Y. Bai, R. Song, K. Xu, and J. An, "An inhomogeneous background imaging method based on generative adversarial network," *IEEE Trans. Microw. Theory Techn.*, vol. 68, no. 11, pp. 4684–4693, Nov. 2020.

[24] S. S. Ahmed, A. Genghammer, A. Schiessl, and L. Schmidt, "Fully electronic *E*-band personnel imager of 2 m^2 aperture based on a multistatic architecture," *IEEE Trans. Microw. Theory Techn.*, vol. 61, no. 1, pp. 651–657, Jan. 2013.

[25] M. T. Ghasr, S. Kharkovsky, R. Bohnert, B. Hirst, and R. Zoughi, "30 GHz linear high-resolution and rapid millimeter wave imaging system for NDE," *IEEE Trans. Antennas Propag.*, vol. 61, no. 9, pp. 4733–4740, Sep. 2013.

[26] M. T. Ghasr, M. J. Horst, M. R. Dvorsky, and R. Zoughi, "Wideband microwave camera for real-time 3-D imaging," *IEEE Trans. Antennas Propag.*, vol. 65, no. 1, pp. 258–268, Jan. 2017.

[27] M. J. Horst, M. T. Ghasr, and R. Zoughi, "A compact microwave camera based on chaotic excitation synthetic-aperture radar," *IEEE Trans. Antennas Propag.*, vol. 67, no. 6, pp. 4148–4161, Jun. 2019.

[28] D. M. Sheen, R. T. Clark, J. Tedeschi, A. M. Jones, and T. E. Hall, "High-resolution 3D microwave imaging of a moving target using optical motion capture," *Proc. SPIE*, vol. 10994, pp. 99–109, May 2019.

[29] Google AI Blog. (Jan. 2021). *Soli Radar-Based Perception and Interaction in Pixel 4*. [Online]. Available: https://ai.googleblog.com/2020/03/soli-radar-based-perception-and.html

[30] Intel RealSense. (Nov. 2020). *Tracking Camera T265*. [Online]. Available: https://www.intelrealsense.com/tracking-camera-t265/

[31] X. Zhuge and A. G. Yarovoy, "Three-dimensional near-field MIMO array imaging using range migration techniques," *IEEE Trans. Image Process.*, vol. 21, no. 6, pp. 3026–3033, Jun. 2012.

[32] J. Yang, J. Thompson, X. Huang, T. Jin, and Z. Zhou, "FMCW radar near field three-dimensional imaging," in *Proc. IEEE Int. Conf. Commun. (ICC)*, Jun. 2012, pp. 6353–6356.

[33] J. Detlefsen, A. Dallinger, S. Schelkshorn, and S. Bertl, "UWB millimeter-wave FMCW radar using hubert transform methods," in *Proc. IEEE 9th Int. Symp. Spread Spectr. Techn. Appl.*, Aug. 2006, pp. 46–48.

[34] OptiTrack. (Nov. 2020). *Optitrack Motion Capture System*. [Online]. Available: http://www.optitrack.com

[35] L. Liu, Q. Chen, Y. Han, H. Xu, J. Li, and B. Wang, "Improved clutter removal by robust principal component analysis for chaos through-wall imaging radar," *Electronics*, vol. 9, no. 1, p. 25, Dec. 2019. [Online]. Available: https://www.mdpi.com/2079-9292/9/1/25
[36] M. Garcia-Fernandez, Y. Alvarez-Lopez, A. Arboleya-Arboleya, F. Las-Heras, Y. Rodriguez-Vaqueiro, B. Gonzalez-Valdes, and A. Pino-Garcia, "SVD-based clutter removal technique for gpr," in *Proc. IEEE Int. Symp. Antennas Propag. USNC/URSI Nat. Radio Sci. Meeting*, Jul. 2017, pp. 2369–2370.

GUILLERMO ÁLVAREZ-NARCIANDI received the M.Sc. degree in telecommunication engineering and the Ph.D. degree from the University of Oviedo, Gijón, Spain, in 2016 and 2020, respectively. He was a Visiting Student with Stanford University, CA, USA, in 2014, a Visiting Scholar with the University of Pisa, Italy, in 2018, and with the Institute of Electronics, Microelectronics and Nanotechnology (IEMN), University of Lille, France, in 2019. His research interests include radar systems and imaging techniques, antenna diagnosis and characterization systems, localization and attitude estimation systems, and RFID technology. He received the AMTA 2019 Student Paper Award (second place) and the Special Award to the Best Entrepreneurship Initiative in the XV Arquímedes national contest in 2017 for the development of a RFID-based location system.

JAIME LAVIADA was born in Gijón, Spain. He received the M.S. degree in telecommunication engineering and the Ph.D. degree from the Universidad de Oviedo, Spain, in 2005 and 2010, respectively. In 2006, he joined the research group Signal Theory and Communications, Universidad de Oviedo, where he has been involved in multiple national and European projects as well as contracts with several companies. In 2015, he moved to the Antennas Group of the Universidad Pública de Navarra with a National Postdoctoral Fellowship collaborating in several applied research projects. Finally, he moved back to the Universidad de Oviedo, where he currently holds a position of Associate Professor. In addition, he has been a Visiting Scholar with the Electromagnetics and Communications Laboratory, Pennsylvania State University, from 2007 to 2008, and with the Applied Microwave NonDestructive Testing Laboratory, Missouri S&T, in 2017. His research interests include numerical techniques applied to EM imaging, antenna measurements, method of moments, and antenna pattern synthesis.

FERNANDO LAS-HERAS (Senior Member, IEEE) received the M.S. and Ph.D. degrees in telecommunication engineering from the Technical University of Madrid (UPM), in 1987 and 1990, respectively. From 1988 to 1990, he was a National Graduate Research Fellow, and from 1991 to 2000, he held a position of Associate Professor with the Department of Signal, Systems and Radio Communications, UPM. Since 2003, he has been held a Full-Professor position with the University of Oviedo, where he was the Vice-Dean for Telecommunication Engineering with the Technical School of Engineering, Gijón, in 2004 to 2008. Since 2001, he has been heading the research group Signal Theory and Communications TSC-UNIOVI with the Department of Electrical Engineering, University of Oviedo. He was a Visiting Lecturer with the National University of Engineering, Peru, in 1996, a Visiting Researcher with Syracuse University, New York, in 2000, and a short-term Visiting Lecturer with ESIGELEC, France, from 2005 to 2011. From 2005 to 2015, he held the Telefónica Chair on "RF Technologies," "ICTs applied to Environment," and "ICTs and Smart cities" with the University of Oviedo. He was a member of the board of directors of the IEEE Spain Section, from 2012 to 2015, member of the board IEEE Microwaves and Antennas Propagation Chapter (AP03/MTT17), from 2016 to 2017, member of the Science, Technology and Innovation Council, Asturias, from 2010 to 2012, and President of the Professional Association of Telecommunication Engineers, Asturias. He has authored scientific articles in the areas of antennas, EM scattering, metamaterials and inverse problems with application to antenna measurement (NF-FF, diagnostics and holography), electromagnetic imaging (security and NDT) and localization, developing computational electromagnetics algorithms and technology on microwaves, millimeter wave, and THz frequency bands.